RSC Advances

ROYAL SOCIETY OF CHEMISTRY

www.rsc.org/advances

In situ fabrication of graphene decorated microstructured globe artichokes of partial molar nickel cobaltite anchored on Ni foam as high-performance supercapacitor electrode

Pinjari Syedvali[b], Gaddam Rajeshkhanna[c], Ediga Umeshbabu[c], Gundla Uday Kiran[b], G Ranga Rao[c], and Ponniah Justin*[a]

Received (in XXX, XXX) Xth XXXXXXXXX 20XX, Accepted Xth XXXXXXXXX 20XX
DOI: 10.1039/b000000x

Abstract

By taking advantage of splendid properties of graphene (electrical conductivity) and transition metal oxides (psuedocapacitance nature), we have in-situ fabricated novel microstructured globe artichokes of rGO/$Ni_{0.3}Co_{2.7}O_4$ composite on nickel foam through a simple surfactant free hydrothermal method followed by calcination process. The globe artichoke flower-like morphology constructed by hundreds of self-assembled micropetals interconnected with several layers and circles at the base to form microspheres of uniform dimension. The as-obtained morphology of microstuctured globe artichokes is enhanced the stability and electrochemical performance of hybrid electrode due to of its unique structures. Therefore, synergetic effects and interconnected structure of thus made binder free rGO/$Ni_{0.3}Co_{2.7}O_4$ hybrid electrode allows better charge transport and exhibiting superb specific capacitance and areal capacitance of 1624 F g^{-1} and 2.37 F cm^{-2} at current density of 2 A g^{-1}. Moreover, the specific capacitance increases from 1088 F g^{-1} to 1728 F g^{-1} at the end of 7000 cycles, which indicates that the material is getting active with cycling. Furthermore, when the power density increased by 16 times i.e. from 0.5 to 8 kW kg^{-1} the energy density sinks to 40 from 56.39 Wh kg^{-1} (i.e., 29 % reduction only), suggesting its remarkable electrochemical performance for the supercapacitor applications.

Keywords: supercapacitors, $NiCo_2O_4$, graphene, hydrothermal, globe artichokes

a Dr. P. Justin*
Department of Chemistry
Rajiv Gandhi University of Knowledge Technologies
RK Valley,Kadapa, 516330, India
E-mail: ponjustin@rgukt.in

b P. Syedvali, G. U. Kiran
Department of Chemical Engineering
Rajiv Gandhi University of Knowledge Technologies
RK Valley,Kadapa, 516330, India

c G. Rajeshkhanna, E. Umeshbabu, Prof. G. Ranga Rao
Department of Chemistry
Indian Institute of Technology Madras
Chennai, 600036, India

†Electronic Supplementary Information (ESI) available: [Additional characterization data including PXRD spectra of graphene oxide, FT-Raman spectra, FT-IR spectra and EDX spectrum of rGO/$Ni_{0.3}Co_{2.7}O_4$ globe artichokes. See DOI: 10.1039/b000000x/].

1. Introduction

Progress in human society, especially modern civilization, has been marked by ever-increasing energy consumption and power requirements. In response to the urgent renewable energy needs of modern society and emerging ecological concerns, it is now essential to develop an effective electrochemical energy conversion and storage systems.[1–3] These technologies will diminish our present dependence on fossil fuels without, causing any harsh consequence on environment.[4–7] Electrochemical capacitor, which is also known as supercapacitor (SC) or ultracapacitor (UC), is a kind of energy storage device, that stores and releases energy within seconds when needed, used to meet the pressing needs of various applications due to its intriguing superior characteristics like high rate of power transmittance, long cycling life, quicker charge and discharge processes, beneficial operating safety and significant potential and so on.[1,3,5–7] Supercapacitors, however, generally provide lower energy density compared to batteries. In spite of its ability to yield lower energy density, supercapacitors have viable representative power access compared to batteries. Conventionally, supercapacitors can be categorized into two different types according to their method of accumulation and release of charge.[1,5] One is Electrochemical Double Layer Capacitors (EDLCs) using activated carbons, carbon aerogels, carbon nanotubes (CNT) and graphene as electrode materials to develop power delivery and energy storage with proportionate to specific capacitance.[8–16] In EDLCs, electrostatic charge accumulated in the Helmholtz double layers at the interface between electrode surface and electrolyte. However, as a consequence of the sole electrostatic surface charging mechanism, these carbon materials suffer from limited specific capacitance and energy density. So EDLCs cannot meet the ever-growing need for peak-power assistance in electric vehicles, and so on.[5] Other type, pseudocapacitors, commonly provides high specific capacitance, in which the mechanism of electrochemical charge storage can be done by faradaic redox reactions on the surface of the electrode.[5,6]

Materials targeted for pseudocapacitors have largely been metal oxides,[17–29] hydroxides,[30,31] sulphides[32,33] and conducting polymers[34–36] because of their multiple oxidation states, which are capable of generating rich redox reactions. These includes Fe_2O_3,[17,18] Bi_2O_3,[19] Co_3O_4,[20,21] MnO_2,[22,23] NiO,[24–27] V_2O_5,[28,29] $Co(OH)_2$,[30] $Ni(OH)_2$,[31] CoS,[32] $NiCo_2S_4$,[33] PEDOT,[34] polyaniline,[35] and polypyrrole[36] etc. However, these electrodes suffer from their constructive disabilities like

capacity degradation, poor cycling rate, and capacity padding towards electrochemical performance.[24] Alternatively many mixed transition metal oxides (MTMOs) such as $NiCo_2O_4$,[37–48] $NiMoO_4$,[49,50] and $LaNiO_3$[51] etc have been explored very recently as effective pseudocapacitance electrode materials than the individual metal oxides. Among MTMOs, spinel $NiCo_2O_4$ possesses at least two order magnitude higher electrical conductivity and better electrochemical activity than individual nickel and cobalt oxides, which originate from the co-existence of the Ni and Co species in $NiCo_2O_4$.[39,40,42,45] Recent work by Lou and his coworkers on partial molar nickel-cobalt oxides clearly shows superior electrochemical activity and a long-term cycling stability which retains 98.1% of its initial capacitance even after 3000 cycles.[45] The electrochemical performance of these pseudocapacitors electrodes were further improved by hybridizing with conducting carbon materials[52–57] or conducting polymers.[58] Such approach can enable versatile and tailor-made properties with performances far beyond those of the individual materials. Considering the feasibility and low cost manufacture procedure, graphene is likely to be perfect alternative electrode compared to carbon nanotubes.[8–10, 15]

In supercapacitor applicaitions, the synthetic method and embedded morphology not merely improve the stability of electrode but also playing key role towards electrochemical performance. Herein, we synthesized 3D microstructured globe artichokes (MGAs) of rGO/$Ni_{0.3}Co_{2.7}O_4$ hybrid electrode associating with reduced graphene oxide and nickel-cobalt oxides, using nickel (Ni) foam as current collector through a simple hydrothermal process. This elegant strategy avoids the dead surfaces of polymer binder and carbon black which are in traditional slurry derived electrode, and thereby improve many competitive benefits such as rich accessible electro active sites, short ion transport pathways and superior electron collection efficiency. Impressively, the synthesized novel electrode exhibits noticeable electrochemical performance with higher capacitance leading to higher energy storage, and cycling performance.

2. Experimental Section

2.1. Preparation of Graphene Oxide (GO)

All chemicals were used in experiment of analytical grade and used for preparation without purification. Graphene oxide was prepared by Modified Hummers method[59] i.e. the concentrated H_2SO_4 (69 mL) was added to a mixture of graphite powder (3.0 g, 1 wt equiv) and $NaNO_3$ (1.5 g, 0.5 wt equiv), and resulting the mixture was cooled using an ice bath to ~10 °C. $KMnO_4$ (9.0 g, 3 wt equiv) was added slowly in portions to keep the reaction temperature below

20 °C. The reaction was warmed to 35 °C and stirred for 7 h. Additional $KMnO_4$ (9.0 g, 3 wt equiv) was added in one portion, and the reaction was stirred for 12 h at 35 °C. The reaction mixture was cooled to room temperature and poured onto ice water (400 mL) with 30% H_2O_2 (3 mL). The mixture underwent centrifugation, decanting and purified by repeated washing using 5% HCl solution, distilled water, followed by ethanol and finally dried at 60 ^oC in vacuum oven for 2 days to give 2.1 g of solid GO product.

2.2. Synthesis of 3D microstructured globe artichokes of rGO/$Ni_{0.3}Co_{2.7}O_4$ on Ni foam

Ni foam (2 cm × 7 cm, 0.4366 g) was pretreated in a 2 M HCl solution in an ultrasound bath for 10 min to remove the surface oxide layer, and then rinsed with deionized water, absolute ethanol and acetone and finally dried at 60 ^oC in vacuum oven for 4 h. And 0.76 g of GO in 80-90 mL of deionized water was sonicated for 15 minutes in room temperature. To this, 2.25 of $Co(NO_3)_2.6H_2O$, 0. 25 g of $Ni(NO_3)_2.6H_2O$, 2.1 g of urea and 0.66 g of NH_4F were added one by one in 10 minutes interval with constant stirring and the resulting solution was made-up to 170 mL by adding deionized water. Subsequently, the above prepared aqueous solution and the pre-treated Ni foam were transferred into a ~210 mL capacity Teflon-lined stainless steel autoclave, sealed, and kept at 160°C for 12 h in muffle furnace at heating rate of 1 $^oC\ min^{-1}$ and then cooled down to room temperature naturally. Finally, the nickel cobalt hydroxyl carbonate precursor with graphene deposited Ni foam was undergone repeated washing using distilled water, followed by ethanol, vacuum dried and then calcined at 400 ^oC in air for 3 h in muffle furnace at heating rate of 1 $^oC\ min^{-1}$ to get crystallized microstructured globe artichokes of rGO/$Ni_{0.3}Co_{2.7}O_4$ composite (deposition weight = 1.48 mg cm^{-2}).

2.3. Physical characterization

Thermogravimetry analysis of precursor sample was performed on TA make TGA Q500V20.10 Build 36 instrument, in air flow (20 mL per min) with linear heating rate of 20 $^{\circ}C$ per min, from room temperature to 800 $^{\circ}C$. The phases and lattice parameters of the samples were characterized by powder X-ray diffraction (PXRD) employing Bruker AXS D8 diffractometer with Cu Kα radiation (λ = 0.15418 nm) operating at 40 kV and 30 mA. The FT-Raman spectrum was taken at room temperature using BRUKER RFS 27 FT-Raman spectrophotometer. FT-IR spectra were recorded in KBr pellets on a JASCO FT-IR-4100 spectrophotometer. Field emission scanning electron microscopy (FESEM) pictures were taken using a FEI Quanta 400 microscope and the basic chemical compositions were determined by

Energy-dispersive X-ray spectroscopy (EDX). The Ni foam coated sample was directly mounted on the carbon tap of the sample holder for SEM analysis. High-resolution TEM (HRTEM) characterization was performed with a JEOL JEM-3010 transmission electron microscopy operated at 200 kV. The sample with Ni foam was sonicated in ethanol for 5 min and the resulting suspension was dropped in a 200 mesh Cu grid for HRTEM analysis. X-ray photoelectron spectroscopy (XPS) analysis was performed with a Specs spectrometer with polychromatic Mg Kα (1253.6 eV) as the photon source with vacuum of 1010 Torr. Nitrogen adsorption and desorption experiments were carried out by Micromeritics ASAP 2020 analyzer. The samples were out gassed at 200 °C for 12 h in a dynamic vacuum before physisorption measurements. The specific surface area was calculated using Brunauer- Emmet-Teller (BET) method, and pore size distribution of the samples was obtained from Barret-Joyner-Halenda (BJH) method.

2.4. Electrochemical characterization

Electrochemical experiments including cyclic voltammetry (CV) chronopotentiometry (CP) and electrochemical impedance spectroscopy (EIS) of the as-prepared electrode were performed on an IVIUMstat electrochemical workstation with a three-electrode experimental setup. The as-prepared hybrid electrode (exposed area 2 × 2 cm^2), platinum foil, and Hg/HgO (CHI Instruments, USA) were used as working, counter and reference electrodes, respectively and all immersed in 2 M KOH aqueous electrolyte. The electrochemical impedance spectra were measured by imposing a sinusoidal alternating voltage frequency of 10^{-2} to 10^5 Hz with amplitude of 5 mV at a constant dc bias potential of 0.3, 0.4 and 0.5 V. The specific and areal capacitances of the self-supported rGO/$Ni_{0.3}Co_{2.7}O_4$ hybrid electrode can be calculated by corresponding equations mentioned below. In addition, to highlighting the electrochemical performance of the electrode, power density, energy density, Coulombic efficiency and capacitance retention/increment have also been calculated.

$$C_s = \frac{1}{mv\Delta V}\int I\,dV \quad (1)$$

$$C_s = \frac{I \times \Delta t}{m \times \Delta V} \quad (2)$$

$$C_a = \frac{I \times \Delta t}{s \times \Delta V} \quad (3)$$

$$E = 0.1389 \times C_s \times (\Delta V)^2 \quad (4)$$

$$P = \frac{E}{\Delta t} \times 3600 \quad (5)$$

$$\eta = \frac{T_d}{T_C} \times 100\ \% \quad (6)$$

$$C_{ret} = \frac{C_s,\text{final}}{C_s,initial} \times 100\ \% \quad (7)$$

$$\tau = \frac{1}{2\pi Z_{img}} \quad (8)$$

where C_s (F g^{-1}) is the specific capacitance, C_a (F cm^{-2}) mentioned for aerial capacitance, m (g) represents the mass of the deposited composition, v (V) refers the scan rate, ΔV (V) stand for potential window, Δt (s) relates to the discharge time, I (A g^{-1}) symbolized for discharge current, s (cm^{-2}) mentioned as surface area of the electrode, E (Wh kg^{-1}) denotes as energy density, P (kW kg^{-1}) named as power density, η accounts for the Coulombic efficiency, τ denotes as time constant, Z_{img} is the frequency corresponding to the maximum of the imaginary component ($Z^{\|}$) of the semicircle, T_d (s) and T_C (s) are discharge time and charge time of the charge discharge curves, C_{ret} pertains for the capacitance retention/increment of the electrode.

3. Results and discussions

3.1. Physicochemical studies

The surface morphology of as synthesized graphene oxide (GO) is evaluated by FESEM and HRTEM. Fig. 1a presents a typical FESEM image of GO which shows a homogeneous wrinkled flake-like morphology of very thin sheet. The PXRD pattern of GO (Fig. S1, ESI†), which also support the same order of overall oxidation. The GO has a diffraction peak centered at 2θ (002) = 9.9° with interplanar spacing of 0.903 nm which is similar to the reported value in the literature,[14,37] showing the complete oxidation of graphite into graphene oxide. Since the interplanar spacing is proportional to the degree of oxidation, the large value of GO is due to the presence of copious hydroxyl, epoxy, and carboxyl groups[14,16]. These functional groups can effectively anchor the metal cations during the hydrothermal reaction conditions. HRTEM micrograph (Fig. 1b) clearly reveals that the GO sheet is very thin, flat and flexible without any cracks which conforms the complete exfoliation of graphite oxide into very few layered GO nanosheets. The GO sheets can be reduced at high pressure and temperatures under hydrothermal

conditions, which has been confirmed by FT Raman and IR spectra (Fig. S2, and S3, ESI†). FT Raman spectra of GO, rGO and rGO/$Ni_{0.3}Co_{2.7}O_4$ composite display similar two broad peaks around ~1300 and 1600 cm^{-1} corresponding to the D and G bands,[37,46] respectively indicating the presence of graphene in the composite. The relative intensity ratio of the D band to the G band (I_D/I_G) in GO as high as 1.04, demonstrating that the chemical reduction altered the structure of GO and introduced a large number of structural defects. [9,12] The oxygenated functional groups of GO like C=O (~1725 cm^{-1}) and C–OH (1391 cm^{-1}) of carboxylic groups, C–O–C (~1043 cm^{-1}) of epoxy groups, and O–H (~3400 cm^{-1}) of hydroxyl groups were also observed in FT-IR spectra as shown in Fig. S3, ESI†.[48,59] It also shows the absorption bands at ~1620 cm^{-1} and ~1240 cm^{-1} which can be attributed to the skeletal vibration of C=C and C–O from unoxidized graphitic domains. Except the skeletal vibration of C=C and C–O bonds, all other oxygenated functional groups are greatly diminished in rGO/$Ni_{0.3}Co_{2.7}O_4$ composite. Two strong peaks at lower frequencies (550 and 653 cm^{-1}) can be assigned respectively, due to the stretching vibrations of the Ni–O and Co–O bonds in $Ni_{0.3}Co_{2.7}O_4$.[48]

Thermal stability of uncalcined samples was investigated by using the thermogravimetric analysis (TGA) recorded from room temperature (RT) to 900 ^oC and the corresponding profiles are presented in Fig. 1c. The three major regular weight losses occurred on the TGA curve between 70 to 420 ^oC. The weight loss before 115 °C were attributed to the removal of the adsorbed water while second weight loss between 115 °C to 265 °C corresponded to removal of an intercalated water, and final weight loss between 265 to 420 ^oC is removal of a structural water along with CO_2 from nickel cobalt hydroxyl carbonate precursor to form spinel nickel cobalt oxide.[45] The temperature beyond 420 ^oC leads to gain in weight, which can be definitely ascribed as the surface oxidation of Ni foam into NiO. Since our sample was calcined at 400 °C, it is utilized to convert the nickel cobalt hydroxyl carbonate precursor into spinel nickel cobalt oxide along with graphene, allowing the lowest temperature to protect against the structural change of Ni foam. The PXRD patterns of calcined samples shows three heavy intense reflections at 45.0°, 52.4°and 76.7°arises from Ni foam as seen from Fig. 1d. For the calcined sample with the exception of the reflections owing to Ni foam, the main peaks are indexed at 2θ = 18.9° (111), 31.1° (220), 36.7° (311), 44.6° (400), 55.4° (422), 59.1° (511) and 64.9° (440) reflections which corresponds to face-centered cubic spinel $Ni_{0.3}Co_{2.7}O_4$ with a space group of Fd3m (JCPDS card no. 73-1702).[39, 44,46,48] In spinel-related structure, the nickel (Ni^{2+}/Ni^{3+})

occupies the octahedral sites while cobalt (Co^{2+}/Co^{3+}) is distributed over both octahedral and tetrahedral sites and oxygen occupies along the faces, [39,40,42] as illustrated in the inset of Fig. 1d. The solid-state redox couples Ni^{2+}/Ni^{3+} and Co^{2+}/Co^{3+} can provide two kinds of active centers for generating pseudocapacitance. [37] The intensity of reflections from spinel $Ni_{0.3}Co_{2.7}O_4$ phase was found to be weak compared to the reflections of Ni foam, which were common phenomenon of Ni foam supported materials [40] and inherent property of face-centered cubic spinel (JCPDS card no. 73-1702).[44–48] Both TGA and PXRD indicate complete transformation of nickel cobalt hydroxyl carbonate precursor into nickel cobalt oxide at 400°C.[41,45] Energy-dispersive X-ray spectroscopy (EDX) also reveals the existence of Co, Ni, O and C species (Fig. S4, ESI†).

More detailed elemental composition and their oxidation state of the rGO/$Ni_{0.3}Co_{2.7}O_4$ are further characterized by X-ray photoelectron spectroscopy (XPS) technique. Fig. 2a represents the deconvolution peaks of C 1s spectra with binding energies of 288.5, 285.8 and 284.5 eV, corresponding to oxygenated carbon species (C=O), C-OH and C=C/C-C, respectively.[16] The core level spectrum of O 1s (Fig. 2b) resolved into three oxygen species which have been marked as O1, O2 and O3.[47] The O1 component observed at low binding energy of 528.9 eV attributed to oxygen bonding with nickel and cobalt (metal-oxygen bond). The O2 component at 531.1 eV attributed to large number of defect sites along with minimum oxygen coordination, with small particles size, whereas, O3 component at 533.1 eV attributed to multiplicity of chemical and physical bonded water at or near the surface of the sample. Fig. 2c shows the Co 2p emission spectrum was best fitted with two spin-orbit doublets, characteristic of Co^{2+} and Co^{3+}, of Co $2p_{1/2}$ and Co $2p_{3/2}$.[40,43,47] The Ni 2p XPS spectrum was also fitted with two spin-orbit doublets (Ni $2p_{1/2}$ and Ni $2p_{3/2}$) which consists Ni^{2+} and Ni^{3+}, and two shakeup satellites (Fig. 2d).[47] Based on the percentage calculations, the oxidation state of Co^{3+} was predominant than Co^{2+}, similarly, the oxidation state of Ni^{3+} also higher than Ni^{2+}. Besides, the total ratio of Co^{3+} + Ni^{3+} to Co^{2+} +Ni^{2+} was found to be 1.93:1. The higher oxidation state is expected to facilitate the fast charge transport across electrode/electrolyte interface. These results conforms that the surface of rGO/$Ni_{0.3}Co_{2.7}O_4$ globe artichokes has composition containing Co^{2+}, Co^{3+}, Ni^{2+} and Ni^{3+}, which is in good accord with the results reported in the literature.[40,42,43,47]

Fig. 3a shows a typical low-magnification FESEM image of rGO/$Ni_{0.3}Co_{2.7}O_4$ composite supported on Ni foam in which the composite uniformly grown with strong adhesion. The as-obtained morphology resembles globe artichokes flowers as shown in Fig. 3b. Fig. 3c and 3d

represents the high-magnification images of rGO/$Ni_{0.3}Co_{2.7}O_4$ composite before and after electrochemical studies, respectively. Both depict large-scale, dense, uniform and well-ordered microstructure globe artichokes flowers perpendicularly grown on skeleton of the Ni foam. Each globe artichokes flower-like structure is composed of hundreds of self-assembled micropetals with several layers. It is noting that each micropetal ranging 5-6 μm length, circles around to form microspheres with huge void spaces between them. The micropetals are interconnected with each other at the centre of the circle and the diameter of micropetals gradually decreases from the base to the tip. The as-obtained MGAs morphology is unique, which is entirely different from other morphologies like nanowires, nanosheets, urchin and dandelion adapted by spinel $NiCo_2O_4$ systems as mentioned in Table 1. Such unique morphology with large open structures favor the fast electrolyte diffusion and the interconnected structures allow charge and electron transportation. Impressively, the globe artichokes morphology of rGO/$Ni_{0.3}Co_{2.7}O_4$ composite still retains its unique original structure after longer 7000 cycles without attenuation (Fig. 3d), which is essential for practical applications of realistic supercapacitor electrodes. This indicates that vigorous charge/discharge processes at vacillate current densities over 7000 cycles does not induce any significant morphological changes.

The MGAs were further characterized by HRTEM and SAED. Fig. 4a–4d shows HRTEM images of rGO/$Ni_{0.3}Co_{2.7}O_4$ composite sample with different magnification which clearly reveals that the micro size globe artichoke flowers constructed by large numbers of long nanorods. The base of the rods ranging 80-90 nm diameters, gradually decrease from the base to the tip. More significantly the nanorods are completely wrapped with rGO thin sheets with smooth surface as seen from Fig. 4c. This type of hybridation could be the most important factor in realizing the synergetic effect between the conducting graphene and the pseudocapacitive oxides. The lattice-resolved TEM image collected at the edge of the nanorods revealed a lattice fringe of 0.241 nm, which is consistent with the d-spacing of (311) plane of the spinel $NiCo_2O_4$ structure.[41,48] Selected area electron diffraction (SAED) pattern of the rGO/$Ni_{0.3}Co_{2.7}O_4$ composite shown in inset of Fig. 4d, which reveals that polycrystalline nature of the sample.[38–40,42, 45–48]

3.3. Electrochemical studies

The as-prepared MGAs of rGO/$Ni_{0.3}Co_{2.7}O_4$ composite electrode underwent cyclic voltammetry (CV) test and the corresponding CV profiles were shown in Fig. 5a with voltage range of -0.2 to 0.6 V, recorded at scan rates of 10, 20 and 30 mV s^{-1} (vs. Hg/HgO). The

oxidation-reduction processes originating from redox couples of Ni^{2+}/Ni^{3+} and Co^{2+}/Co^{3+} due to the insertion and de-insertion of OH^- ions.[37] This suggests that the charge storage mechanism of the composite electrode constitutes a strong pseudocapacitive nature that is different from that of the electric double layer capacitance which is usually close to ideal rectangular shapes.[1,8,10,11,13,16] With the increasing scan rate, the oxidation and reduction peaks shifted toward higher and lower potentials, respectively, with a large potential separation leading to increased redox current. At higher scan rates, the effective diffusion of electrolyte ion to inner active sites of electrode is greatly reduced, which led to unsymmetric CV profiles.[39,46] The effect of scan rates (Fig. 5b) can be investigated through calculating the specific capacitance (Equation 1) at sequential scan rates ranging from 10 to 100 mV s^{-1}. The specific capacitance of the rGO/$Ni_{0.3}Co_{2.7}O_4$ electrode at scan rates of 10, 20, 30, 40, 50, and 70 mV s^{-1} can calculated to be 1805, 1308, 1050, 885, 772 and 618 F g^{-1}, respectively. The hybrid rGO/$Ni_{0.3}Co_{2.7}O_4$ electrode owns a significantly larger specific capacitance than individual nickel or cobalt oxides/hydroxides/sulphides.[20,21,24–27,30,32] The lower specific capacitance values normally observed at higher scan rates because these are associated with the resistances and devious diffusion tracts within the matrix of the electrode material. At higher scan rates, only outer regions can be accessed by the ions whereas at lower scan rates both outer and inner pore surfaces are employed for charge propagation.[24, 25,44–48]

The chronopotentiometry test was conducted as-prepared rGO/$Ni_{0.3}Co_{2.7}O_4$ hybrid electrode with potential range of 0.0 V to 0.5 V. Fig. 5c depicts the galvanostatic charge-discharge curves of the hybrid electrode at different current densities. The specific capacitance (C_s) and areal capacitance (C_a) of the rGO/$Ni_{0.3}Co_{2.7}O_4$ electrode (Fig. 5d) are calculated using the mentioned equations (Equations 3 and 4) at current densities ranging from 2 to 32 A g^{-1}. The highest specific capacitance 1624 F g^{-1} (C_a = 2.37 F cm^{-2}) recorded at 2 A g^{-1}. Subsequently, the C_s values are 1536 (2.24 F cm^{-2}), 1376 (2 F cm^{-2}), 1536 (2.24 F cm^{-2}), 1344 (1.96 F cm^{-2}) and 1152 F g^{-1} (1.68 F cm^{-2}) at current densities of 4, 8, 16, 24 and 32 A g^{-1}, respectively. Basically, the hydrated OH^- ions transferred from electrolyte to electrode surface during charging process while in discharging process, the movement of OH^- ions is quite reversed. In general, the insertion of hydrated ions on the electrode surface is corresponding to the time to reach the OH^- ions onto the surface of electrode at respective lower/higher current densities. Accordingly, the incomplete electrode surface, with hydrated ions, is leads to decrease in specific/areal

capacitance.[24,25,37] However, in this study the ~18% reduction of the specific capacitance is not very significant when the discharge current is increased from 2 to 24 A g^{-1}. Since higher discharge currents are applied in the large scale practical applications, the present featured electrodes were advisable rather than poor electrochemical performance electrodes.

To evaluate long time stability of MGAs rGO/$Ni_{0.3}Co_{2.7}O_4$ hybrid electrode for supercapacitors applications, a galvanostatic charge/discharge measurements were carried out at vacillate current densities ranging from 8 to 32 A g^{-1} and reverse to 8 A g^{-1} in 7000 cycles. Both C_s and C_a were calculated at each 50th cycle interval of 7000 cycles and presnted in Fig. 6a. The current density of 8 A g^{-1} (12 mA cm^{-2}) applied for initial 500 cycles that results in specific and areal capacitances gradually increases, from 1088 F g^{-1} and 1.58 F cm^{-2} , up to 1376 F g^{-1} and 2.008 F cm^{-2}. The increasing capacitance is attributed to the full activation of the electrode that enhances the number of the active sites on the surface of electrode and allows the immobilized ions to gradually diffuse out into the electrolyte.[38,40,42,50] Subsequently, the current density increased stepwise to 16 A g^{-1} (24 mA cm^{-2}), the specific and areal capacitances of the rGO/$Ni_{0.3}Co_{2.7}O_4$ hybrid electrode is 1536 F g^{-1} and 2.24 F cm^{-2}, which is slowly decreased to 1344 F g^{-1} and 1.96 F cm^{-2} at 24 A g^{-1} (36 mA cm^{-2}) and 1152 F g^{-1} and 1.68 F cm^{-2} at 32 A g^{-1} (48 mA cm^{-2}), respectively. After 4500 cycles, the current rate again reduced back step by step to 24 A g^{-1} (36 mA cm^{-2}) where specific and areal capacitances of 1248 F g^{-1} and 1.82 F cm^{-2}, 1472 F g^{-1} and 2.15 F cm^{-2} at 16 A g^{-1} (24 mA cm^{-2}), finally 1728 F g^{-1} and 2.52 F cm^{-2} at 8 A g^{-1} (12 mA cm^{-2}) are recovered, respectively. The outstanding increment of specific capacitance (C_{ret}) can be observed in Fig. 6b which reveals that it would extensively maintained more than 100 % throughout 7000 cycles at vacillating current densities. More interestingly it specific capacitance increases from 1088 F g^{-1} to 1728 F g^{-1} from 2nd to 7000th cycle at a current density of 8 A g^{-1}, which are superior performances than most of the literatures (Table 1). Even at very high current density of 16 A g^{-1}, 24 A g^{-1} and 32 A g^{-1} still there is an increment of specific capacitance of ~35 %, ~15 % and ~5 % respectively from the initial value of 1088 F g^{-1}, instead of decreasing as in most stability cycle tests reported for spinel $NiCo_2O_4$ electrodes.[38–40, 42–48] As shown in Fig. 6b, interestingly, the Coulombic efficiency maintained more than 100 % where highest value is shown ~128.5 % and least value of ~102.4 % at current densities of 32 A g^{-1} and 8 A g^{-1}, respectively. The higher Coulombic efficiency at higher current density conditions signifies lower internal resistance, shorter ion transport distances and better electroactive surface

utilization due to insignificant structural deformation and phase transformation even up to very long 7000 cycles. Electrochemical impedance spectroscopy (EIS) measurements have been performed in order to evaluate the microstructure and electrochemical properties of as-prepared MGAs of rGO/$Ni_{0.3}Co_{2.7}O_4$ composite electrode. The Nyquist plots of EIS measured at different potentials are displayed in Fig. 6c. This study shows that the charge-transfer resistance (R_{ct}) in this electrode is 0.075 Ω cm^{-2}, which is much lower than the values reported for $NiCo_2O_4$,[39,46] and other materials.[22,24–27,49,50] Moreover, from the frequency corresponding to the maximum of the imaginary component of the semicircle, the time constant (τ) was estimated to be ~12 ms. Further, the electrical conductivity of rGO/$Ni_{0.3}Co_{2.7}O_4$ composite was measured by four-point probe method and estimated to be ~ 0.97s cm^{-1}. This can be definitely ascribed to the better enhanced electronic conductivity of rGO/$Ni_{0.3}Co_{2.7}O_4$ electrode in accord with the galvanostatic charge/discharge results as discussed above. The deviation from near 90° is along the imaginary axis much larger when bias potential is decreased from 0.5 to 0.3 V. The deviation from the near 90° along the imaginary axis is attributed to the redox-related charge storage mechanism of rGO/$Ni_{0.3}Co_{2.7}O_4$ electrode. The energy (E) and power densities (P) were calculated from galvanostatic discharge curves using the equations (Equations 4, 5) and plotted Ragone plot (Fig. 6d). The rGO/$Ni_{0.3}Co_{2.7}O_4$ composite electrode exhibits an impressive high energy and power densities which stands almost linear nature. To the noting, the maximum energy density of as-obtained hybrid electrode presents higher energy density is 56.39 Wh kg^{-1} with power density of 500 W kg^{-1} at 2 A g^{-1}. With the increasing power densities of 1000 (4 A g^{-1}), 2000 (8 A g^{-1}), 4000 (16 A g^{-1}), 6000 (24 A g^{-1}) and 8000 W kg^{-1} (32 A g^{-1}) the energy density can reach 53.33, 47.78, 53.33, 46.67 and 40 Wh kg^{-1}, respectively. Remarkably, when the power density increased by 16 times i.e. from 0.5 to 8 kW kg^{-1} the energy density sinks to 40 from 56.39 Wh kg^{-1} (i.e., 29 % reduction only) and is still larger than most of the reported values.[38,45,49,50] This promising results suggesting that MGAs of rGO/$Ni_{0.3}Co_{2.7}O_4$ hybrid electrode is highly assuring prospect as supercapacitor electrodes for real or practical applications.

The preparation process of microstructured globe artichokes rGO/$Ni_{0.3}Co_{2.7}O_4$ composite electrode is clearly illustrated in Scheme 1. Typically, the MGAs of rGO/$Ni_{0.3}Co_{2.7}O_4$ was directly grown on conducting Ni foam with strong adhesion which allows intimate contacts and effective electron transport between them and charge collecting Ni foam substrate resulting

robust cycling performances. There are numerous mesopores in the rGO/$Ni_{0.3}Co_{2.7}O_4$ composite surface alleviating the diffusion of electrolyte ions and providing to a great extent of active sites to take part in charge transfer reactions. This can be further conformed by specific surface area and corresponding BJH pore size distribution plots as shown in Fig. S5, ESI†. These isotherms can be categorized as "type IV" with H3 type hysteresis loops.[32,48] It has a pore volume as high as 0.3 cm^3 g^{-1} with distribution of pores in the mesoporous range of 2-47 nm with maxima at around 2.7 nm and 18.4 nm (BJH Desorption average pore radius is 4.6 nm). These features would be important in enhancing the transport and diffusion phenomenon of electrolyte ions during the charge/discharging processes. Moreover, the globe artichokes microstructures formed by self-assembling of nanorods with large open spaces between the neighboring petals/flowers (Fig. 3), which allows easily assessing of electrolyte without any hindrance, that leading to high rate capability and good power performances. In addition, graphene sheets over the petals (Fig. 4c) of globe artichokes could buffer the volume change of $Ni_{0.3}Co_{2.7}O_4$ that leads to the volume expansion during the rapid charge/discharge process, which is encouraging to getting better cyclic performance and also contributing electrical double-layer capacitance to the overall specific capacitance. As seen from the TEM images there is an effective hybridization of $Ni_{0.3}Co_{2.7}O_4$ with graphene which is crucial for enhancing the advanced functions, as it can enable versatile and tailor-made properties with performances far beyond those of the individual materials. Finally, partial molar nickel-cobalt oxides ensure that sufficient faradaic reactions can occur at high current densities for energy storage and power delivery. All of the above characteristics in turn contribute to the superior electrochemical performance of the rGO/$Ni_{0.3}Co_{2.7}O_4$ composite electrode.

4. Conclusion

In summary, novel 3D microstructured globe artichokes formed by reduced graphene oxide along with partial molar nickel-cobalt oxides (rGO/$Ni_{0.3}Co_{2.7}O_4$) grown over Ni foam successfully for the first time by simple hydrothermal method. The 3D MGAs were made by self-assembling nanorods, and each nanoroads were wrapped by reduced graphene oxide nanosheets. To have such preferential lineaments, as-obtained rGO/$Ni_{0.3}Co_{2.7}O_4$ hybrid electrode was able to produce ultrahigh specific capacitance of 1624 and 1344 F g^{-1} at current densities of 2 and 24 A g^{-1}. Remarkably, when the areal current densities increases by 16 times (i.e., 3 to 36 mA cm^{-2}) the areal capacitance only sinks to 1.96 F cm^{-2} from 2.37 F cm^{-2} (i.e., only 17 %

reduction), which conforms its higher rate and power capability. In long time stability test, as-obtained rGO/$Ni_{0.3}Co_{2.7}O_4$ hybrid electrode exhibits an excellent cycle profile with a Coulombic efficiency more than 100% throughout 7000 cycles with good loading (rGO/$Ni_{0.3}Co_{2.7}O_4$ deposition weight = 1.48 mg cm^{-2}). At the end of 7000 cycles its specific capacitance increases up to ~159 % from its initial value at a current density of 8 A g^{-1}, which indicates that the material is getting active with cycling. In this work, four elegant design strategies like interconnected nanorods, manipulation of compositions, effective hybridization between conducting graphene and the pseudocapacitive oxides, and easy fabrication of electrode over 3D conductive substrate of Ni foam were adapted through a single step hydrothermal route inorder to maximize the electrochemical performances. These design strategies are not only for supercapacitors electrodes but also is desirable in the design of other electrochemical applications like alkaline fuel cells, Li-ion batteries, Na-ion batteries and biosensor applications with excellent performances.

Acknowledgements

P. Syedvali, G. U. Kiran, Dr. P. Justin acknowledge the Rajiv Gandhi University of Knowledge Technologies (RGUKT) for providing IVIUMstat electrochemical workstation. We also gratefully acknowledge the DST-FIST facilities in IIT Madras for physical characterization of materials and Alternative Energy and Nanotechnology Laboratory (AENL) for XPS characterization.

References

1 B. E. Conway, *Electrochemical Supercapacitors*: *Scientific Fundamentals and Technological Applications*, Kluwer Academic/Plenum Publishers, New York 1999.

2 A. S.Aricò, P. Bruce, B. Scrosati, J.-M. Tarascon and W. V. Schalkwijk, *Nat. Mater.*, 2005, **4**, 366.

3 Y.-G. Guo, J.-S. Hu and L.-J. Wan, *Adv. Mater.*, 2008, **20**, 2878.

4 J. R. Miller and P. Simon, *Science*, 2008, **321**, 651.

5 P. Simon and Y. Gogotsi, *Nat. Mater.*, 2008, **7**, 845.

6 Q. L. Lu, J. G. Chen and J. Q. Xiao, *Angew. Chem. Int. Ed.*, 2013, **52**, 1882.

7 P. Simon, Y. Gogotsi and B. Dunn, *Science*, 2014, **343**, 1210.

8 S. R. C. Vivekchand, C. S. Rout, K. S. Subrahmanyam, A. Govindaraj and C. N. R. Rao, *J.Chem. Sci.*, 2008, **120**, 9.

9 Y. Zhu, S. Murali, W. Cai, X. Li, J. W. Suk, J. R. Potts and R. S. Ruoff, *Adv. Mater*., 2010, **22**, 3906.

10 Y. Zhu, S. Murali, M. D. Stoller, K. J. Ganesh, W. Cai, P. J. Ferreira, A. Pirkle, R. M. Wallace, K. A. Cychosz, M. Thommes, D. Su, E. A. Stach and R. S. Ruoff, *Science*, 2011, **332**, 1537.

11 L. Dai, D. W. Chang, J.-B. Baek and W. Lu, *Small*, 2012, **8**, 1130.

12 N. Jha, P. Ramesh, E. Bekyarova, M. E. Itkis and R. C. Haddon, *Adv. Energy Mater*., 2012, **2**, 438.

13 M. G. Hahm, A. L. M. Reddy, D. P. Cole, M. Rivera, J. A. Vento, J. Nam, H. Y. Jung, Y. L. Kim, N. T. Narayanan, D. P. Hashim, C. Galande, Y. J. Jung, M. Bundy, S. Karna, P. M. Ajayan and R. Vajtai, *Nano Lett*., 2012, **12**, 5616.

14 M. M. Hantel, T. Kaspar, R. Nesper, A. Wokaun and R. Kötz, *Chem. Eur. J.* 2012, **18**, 9125.

15 L. Dong, Z. Chen, D Yang and H Lu, *RSC Ad v*., 2013, **3**, 21183.

16 J.-S. Lee, S.-I Kim, J.-C. Yoon and J.-H. Jang, *ACS Nano*, 2013, **7**, 6047.

17 S.-Y. Wang and N.-L. Wu, *J. Appl. Electrochem*., 2003, **33**, 345.

18 N.-L. Wu, S.-Y. Wang, C.-Y. Han, D.-S. Wu and L.-R. Shiue, *J. Power Sources*, 2003, **113**, 173.

19 F.-L. Zheng, G.-R. Li, Y.-N. Ou, Z.-L. Wang, C.-Y. Su and Y.-X. Tong, *Chem. Commun*., 2010, **46**, 5021.

20 S. K. Meher and G. Ranga Rao, *J. Phys. Chem. C*, 2011, **115**, 15646.

21 G. Wang, H. Liu, J. Horvat, B. Wang, S. Qiao, J. Park and H. Ahn, *Chem. Eur. J*, 2010, **16**, 11020.

22 P. Ragupathy, D. H. Park, G. Campet, H. N. Vasan, S.-J. Hwang, J.-H. Choy and N. Munichandraiah, *J. Phys. Chem. C*, 2009, **113**, 6303.

23 Y. Munaiah, B. G. S. Raj, T. P. Kumar and P. Ragupathy, *J. Mater. Chem. A*, 2013, **1**, 4300.

24 P. Justin, S. K. Meher and G. Ranga Rao, *J. Phys. Chem. C*, 2010, **114**, 5203.

25 S. K. Meher, P. Justin and G. Ranga Rao, *Nanoscale*, 2011, **3**, 683.

26 B. Wang , J. S. Chen , Z. Y. Wang, S. Madhavi and X. W. Lou, *Adv. Energy Mater*., 2012, **2**, 1188.

27 S. Vijayakumar, S. Nagamuthu and G. Muralidharan, *ACS Appl. Mater. Interfaces*, 2013, **5**, 2188.

28 G. Wee, H. Z. Soh, Y. L. Cheah, S. G. Mhaisalkar and M. Srinivasan, *J. Mater. Chem.*, 2010, **20**, 6720.

29 K. Jeyalakshmi, S. Vijayakumar, S. Nagamuthu and G. Muralidharan, *Mater. Res. Bull.*, 2013, **48**, 760.

30 S. Chou, J. Wang, H. K. Liu and S. X. Dou, *J. Electrochem. Soc.*, 2008, **155**, A926.

31 W. Zhou, M. Yao, L. Guo, Y. Li, J. Li and S. Yang, *J. Am. Chem. Soc.*, 2009, **131**, 2959.

32 P. Justin and G. Ranga Rao, *Int. J. Hydrogen Energy*, 2010, **35**, 9709.

33 Y. Zhang, M. Ma, J. Yang, C. Sun, H. Su, W. Huang and X. Dong, *Nanoscale*, 2014, **6**, 9824.

34 R. Liu, S. I. Cho and S. B. Lee, *Nanotechnology*, 2008, **18**, 215710.

35 F. Montilla, M. A. Cotarelo and E. Morallón, *J. Mater. Chem.*, 2009, **19**, 305.

36 Y. Shi, L. Pan, B. Liu, Y. Wang, Y. Cui, Z. Bao and G. Yu, *J. Mater. Chem. A*, 2014, **2**, 6086.

37 H.-Wen Wang, Z.-Ai Hu, Y.-Q. Chang, Y.-L. Chen, H.-Y. Wu, Z.-Y. Zhang and Y.-Y. Yang, *J. Mater. Chem.*, 2011, **21**, 10504.

38 H. Jiang, J. Ma and C. Li, *Chem. Commun.*, 2012, **48**, 4465.

39 Q. F. Wang, B. Liu, X. F. Wang, S. H. Ran, L. M. Wang, D. Chen and G. Z. Shen, *J. Mater. Chem.*, 2012, **22**, 21647.

40 C. Z. Yuan, J. Y. Li, L. R. Hou, X. G. Zhang, L. F. Shen and X. W. Lou, *Adv. Funct. Mater.*, 2012, **22**, 4592.

41 J. Chang, J. Sun, C. Xu, H. Xu and L. Gao, *Nanoscale*, 2012, **4**, 6786.

42 L. F. Shen, Q. Che, H. S. Li and X. G. Zhang, *Adv. Funct. Mater.*, 2013, **24**, 2630.

43 R. Zou, K. Xu, T. Wang, G. He, Q. Liu, X. Liu, Z. Zhang and J. Hu, *J. Mater. Chem. A*, 2013, **1**, 8560.

44 J. Du, G. Zhou, H. Zhang, C. Cheng, J. Ma, W. Wei, L. Chen and T. Wang, *ACS Appl. Mater. Interfaces*, 2013, **5**, 7405.

45 H. B. Wu, H. Pang and X. W. Lou, *Energy Environ. Sci.*, 2013, **6**, 3619.

46 N. Padmanathan and S. Selladurai, *RSC Adv.*, 2014, **4**, 8341.

47 J. Liang, Z. Fan, S. Chen, S. Ding and G. Yang, *Chem. Mater.*, 2014, **26**, 4354.

48 E. Umeshbabu, G. Rajeshkhanna and G. Ranga Rao, *Int. J Hydrogen Energy*, 2014, **39**, 15627.

49 D. Ghosh, S. Giri and C. K. Das, *Nanoscale*, 2013, **5**, 10428.

50 B. Senthilkumar, K. V. Sankar, R. K. Selvan, M. Danielle and M. Manickam, *RSC Adv*., 2013, **3**, 352.

51 D. K. Hwang, S. Kim, J.-H. Lee, I.-S. Hwang and I.-D. Kim, *J. Mater. Chem*., 2011, **21**, 1959.

52 S. Chen, J. Zhu, X. Wu, Q. Han and X. Wang, *ACS Nano* 2010, **4**, 2822.

53 H. Wang, H. S. Casalongue, Y. Liang and H. Dai, *J. Am. Chem. Soc*., 2010, **132**, 7472.

54 Q. Wu, Y. Xu, Z. Yao, A. Liu and G. Shi, *ACS Nano*, 2010, **4**, 1963.

55 S. D. Perera , B. Patel , N. Nijem , K. Roodenko , O. Seitz , J. P. Ferraris , Y. Chabal and K. J. Balkus Jr., *Adv. Energy Mater*., 2011, **1**, 936.

56 K. Wang, X. Ma, Z. Zhang, M. Zheng, Z. Geng and Z. Wang, *Chem. Eur. J*, 2013, **19**, 7084.

57 C. Shang, S. Dong, S. Wang, D. Xiao, P. Han, X. Wang, L. Gu and G. Cui, ACS Nano, 2013, **7**, 5430.

58 Q. Qu, Y. Zhu, X. Gao and Y. Wu, *Adv. Energy Mater*., 2012, **2**, 950.

59 D. C. Marcano, D. V. Kosynkin, J. M. Berlin, A. Sinitskii, Z. Sun, A. Slesarev, L. B. Alemany, W. Lu and J. M. Tour, *ACS Nano*, 2010, **4**, 4806.

Table 1. Summary of recent research results of spinel $NiCo_2O_4$ for supercapacitor electrodes.

Preparation Method	Current Collector	Morphology	Cs [F/g] @ *i* [A/g][a)]	Energy Density [Wh/kg]	Power Density [W/kg]	Capacity Retention (cycles)	Ref & Year
Precipitation[b)]	Ni foam	Nanosheets	835 @ 1 615 @ 20	—	—	113.5 % (4000)	37, 2011
Soft Template	graphite paper	Nanowires	743 @ 1 584 @ 40	22.6	219	93.8 % (3000)	38, 2012
Hydrothermal	Ni foam	Urchin-like nanostructures	1650 @ 1 1348 @ 15	—	—	91.8 % (2000)	39, 2012
Electrodeposition	Ni foam	Nanosheets	2010 @ 2 1450 @ 20	—	—	94 % (2400)	40, 2012
Hydrothermal	Ni foam	Nanowires	1283 @ 1 1010 @ 20	—	—	98 % (5000)	42, 2013
Hydrothermal	Ni foam	Chain-like Nanowires	1284 @ 1 986 @ 20	—	—	~97.5 % (3000)	43, 2013
Electrodeposition	Carbon fiber	Nanosheets	2658 @ 2 1866 @ 20	—	—	80 % (3000)	44, 2013
Precipitation[c)]	Ni grid	Dandelion	960 @ 0.625 805 @ 6.25	27.1	141	98.1 % (3000)	45, 2013
Hydrothermal	Carbon fiber	Nanowall-network	1225 @ 5 996 @ 40	—	—	87 % (2000)	46, 2014
Facile Preparation	Graphite paper	Nanosheets	1886.6 @ 6 1500 @ 30	—	—	94.7 % (8600)	47, 2014
Hydrothermal	Ni foil	Urchin-like	636 @ 0.5 445.2 @ 16	34.6	958	70 % (1000)	48, 2014
Hydrothermal[d)]	Ni foam	Globe artichoke flowers	1624 @ 2 1152 @ 32	56.39	500	~159 % (7000)	This work, 2015

[a)] Specific capacitance (C_s) at minimum and maximum current densities calculated from discharge curves, respectively; [b)] RGO-$NiCo_2O_4$; [c)] $Ni_{0.3}Co_{2.7}O_4$; [d)] rGO/$Ni_{0.3}Co_{2.7}O_4$.

Fig. 1 (a) FESEM and (b) HRTEM images of as-synthesized GO. (c) TGA profile of uncalcined precursor. (d) PXRD pattern of rGO/$Ni_{0.3}Co_{2.7}O_4$ composite grown over Ni foam.

Fig. 2 Core level XPS spectra of (a) C 1s, (b) O 1s, (c) Co 2p and (d) Ni 2p for the rGO/$Ni_{0.3}Co_{2.7}O_4$ composite synthesized over the Ni foam.

Fig. 3 (a) Low magnification FESEM image of Ni foam covered with rGO/$Ni_{0.3}Co_{2.7}O_4$ composite. (b) Schematic diagram of natural globe artichoke flowers. (c,d) FESEM images of microstructured globe artichokes of rGO/$Ni_{0.3}Co_{2.7}O_4$ composite before and after 7000 cycles, respectively.

Fig. 4 HRTEM images at different resolutions (a) 500 nm, (b) 100 nm, (c) 20 nm and (d) 5 nm (inset: SAED pattern) of microstructured globe artichokes of rGO/$Ni_{0.3}Co_{2.7}O_4$ composite.

Fig. 5 (a) CV curves of first three scan rate, (b) Effect of scan rates, (c) Charge-discharge curves of rGO/$Ni_{0.3}Co_{2.7}O_4$ composite electrode. (d) Specific capacitance and areal capacitances of charge-discharge curves at various current densities ranging from 2 to 32 A g^{-1}.

Fig. 6 (a) The cyclic performances of rGO/$Ni_{0.3}Co_{2.7}O_4$ hybrid electrode at progressive current density throughout 7000 cycles. (b) Cyclic performance of capacitance retention (%) and Coulombic efficiency (%). (c) Electrochemical impedance spectra after 500 cycles of galvanostatic charge-discharge process (inset: equivalent circuit for fitting). (d) Ragone plot of as-prepared hybrid electrode along with reference.[45]

Scheme 1 (i), (ii), and (iii) Preparation illustration of microstructure rGO/$Ni_{0.3}Co_{2.7}O_4$ globe artichokes hybrid electrode. (iv) OH^- ions movement onto Ni foam matrix during charging and discharging.

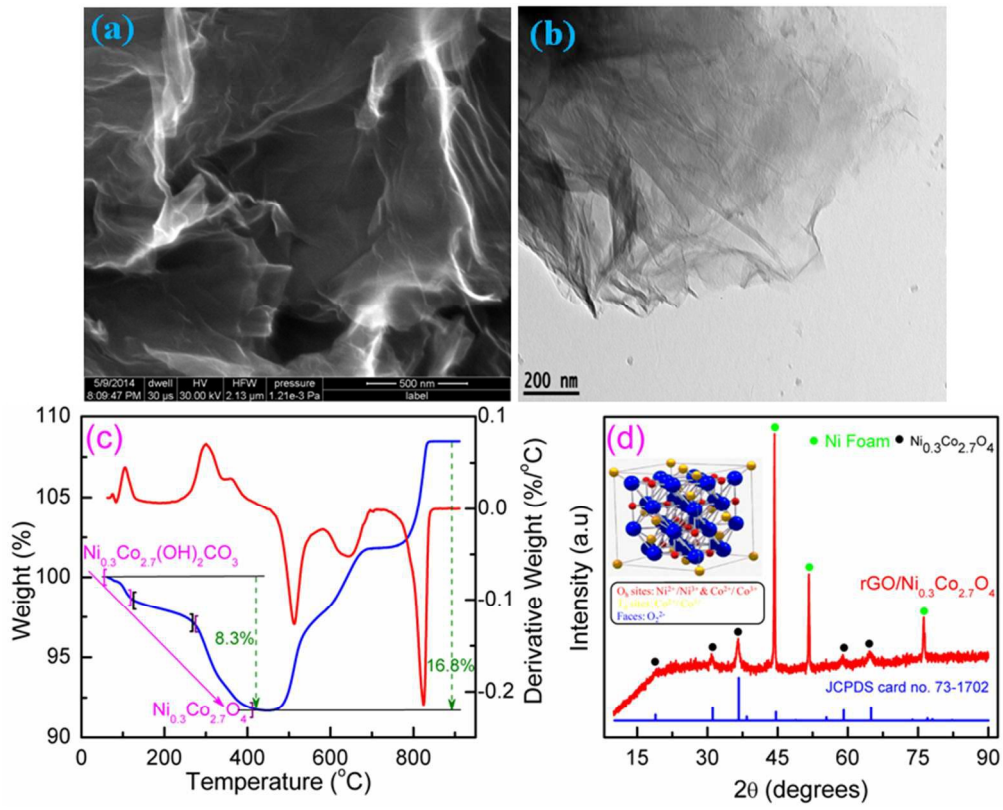

Fig. 1 (a) FESEM and (b) HRTEM images of as-synthesized GO. (c) TGA profile of uncalcined precursor. (d) PXRD pattern of rGO/Ni0.3Co2.7O4 composite grown over Ni foam.
228x183mm (96 x 96 DPI)

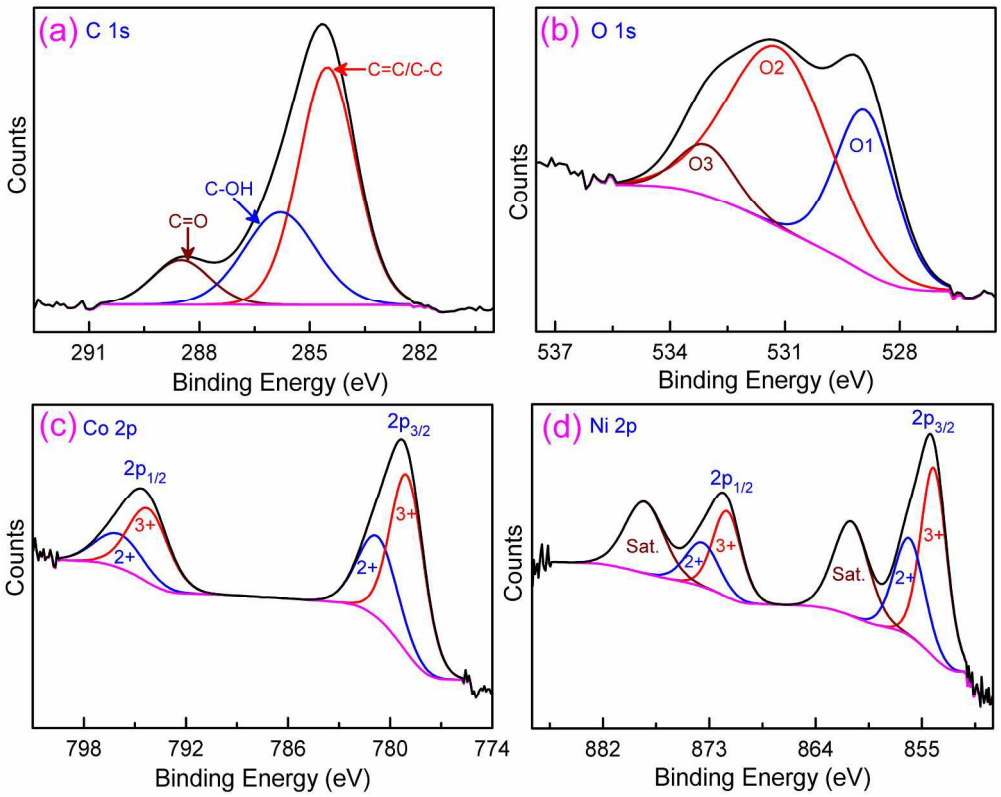

Fig. 2 Core level XPS spectra of (a) C 1s, (b) O 1s, (c) Co 2p and (d) Ni 2p for the rGO/Ni0.3Co2.7O4 composite synthesized over the Ni foam.
232x183mm (300 x 300 DPI)

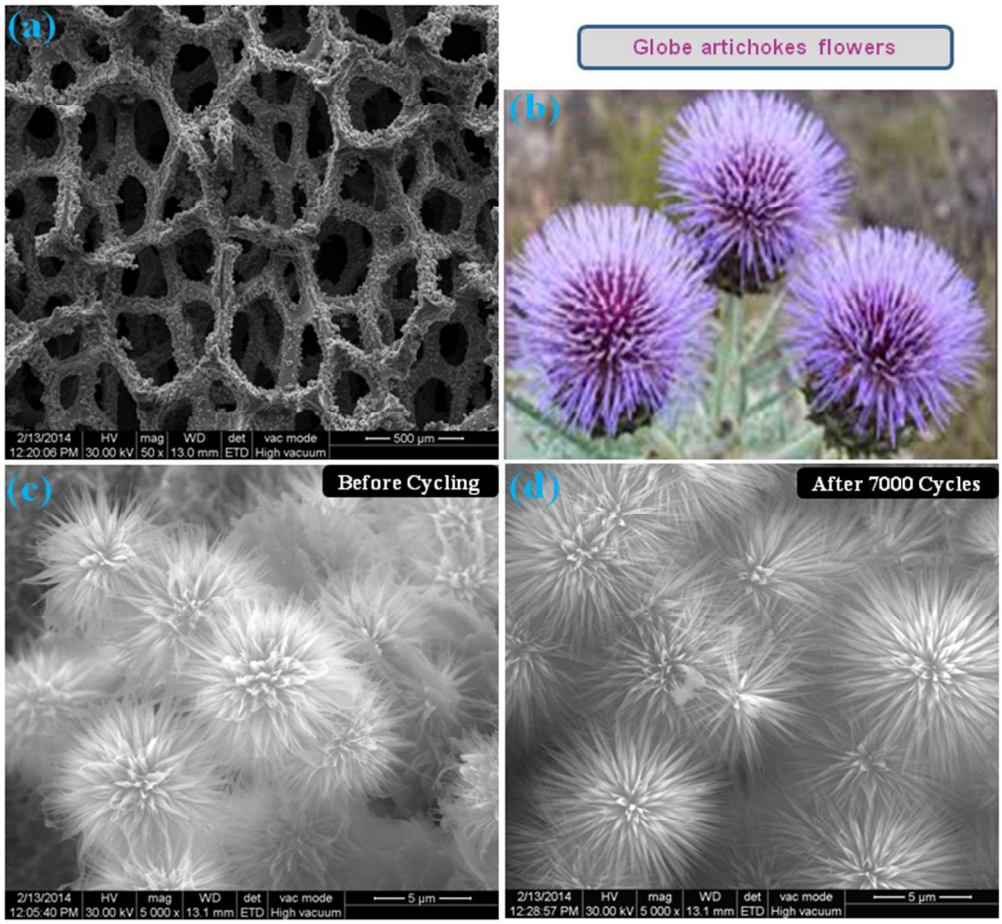

Fig. 3 (a) Low magnification FESEM image of Ni foam covered with rGO/Ni0.3Co2.7O4 composite. (b) Schematic diagram of natural globe artichoke flowers. (c,d) FESEM images of microstructured globe artichokes of rGO/Ni0.3Co2.7O4 composite before and after 7000 cycles, respectively.
206x189mm (96 x 96 DPI)

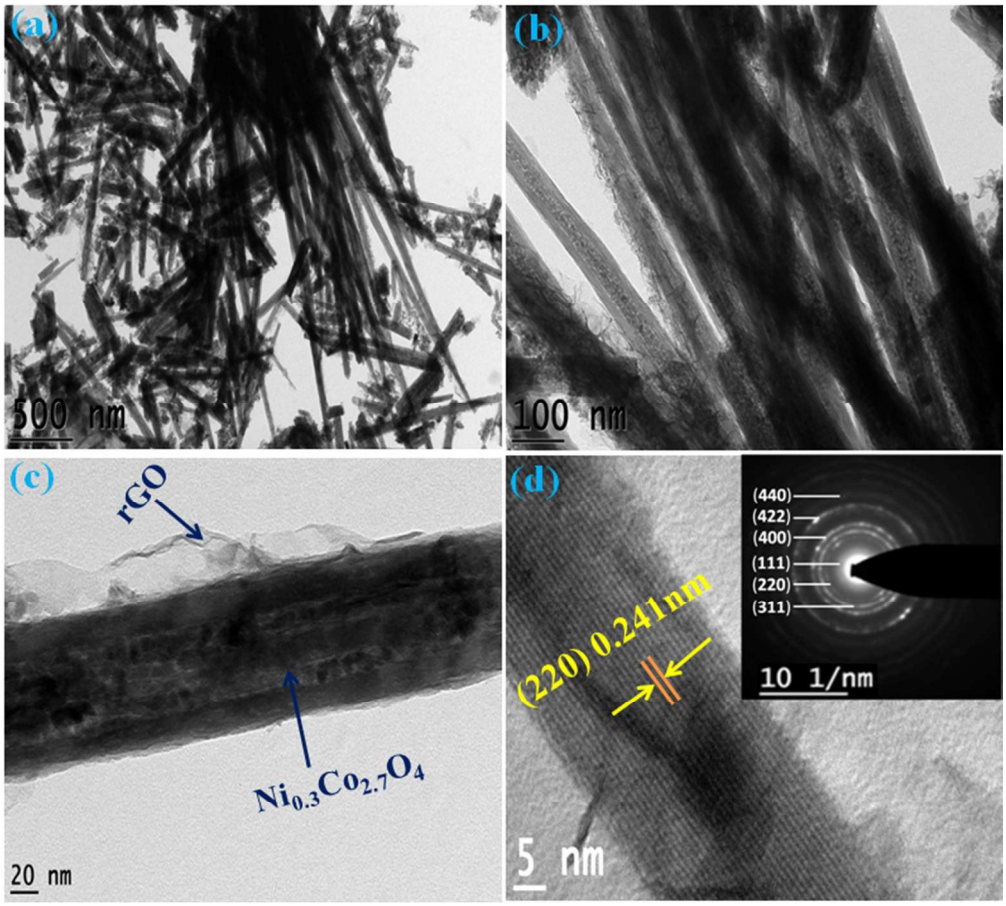

Fig. 4 HRTEM images at different resolutions (a) 500 nm, (b) 100 nm, (c) 20 nm and (d) 5 nm (inset: SAED pattern) of microstructured globe artichokes of rGO/Ni0.3Co2.7O4 composite.
209x188mm (96 x 96 DPI)

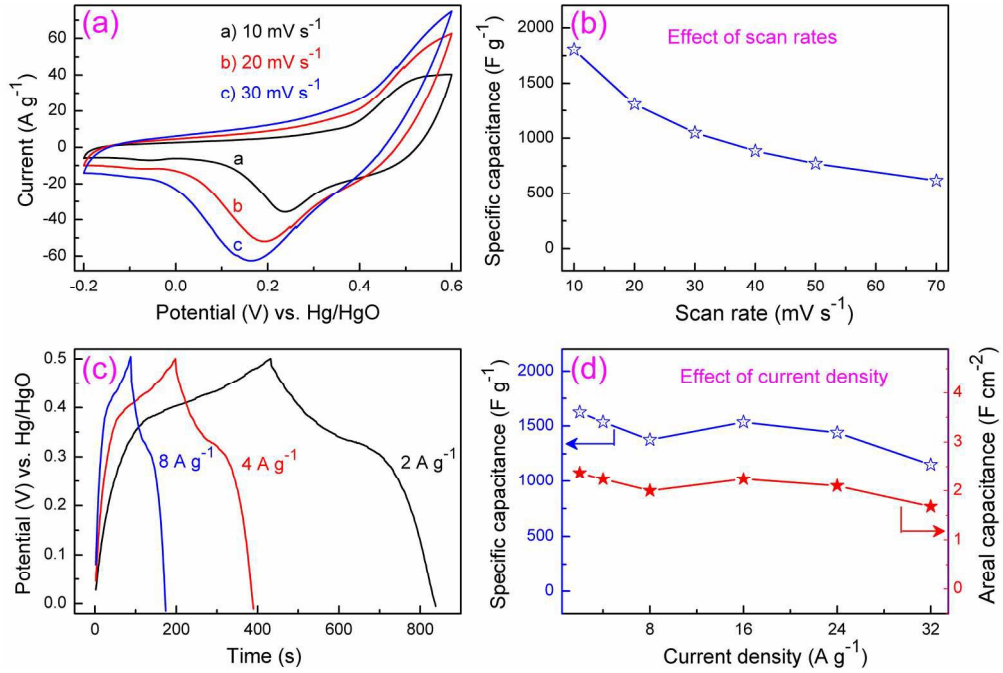

Fig. 5 (a) CV curves of first three scan rate, (b) Effect of scan rates, (c) Charge-discharge curves of rGO/Ni0.3Co2.7O4 composite electrode. (d) Specific capacitance and areal capacitances of charge-discharge curves at various current densities ranging from 2 to 32 A g-1.
194x129mm (300 x 300 DPI)

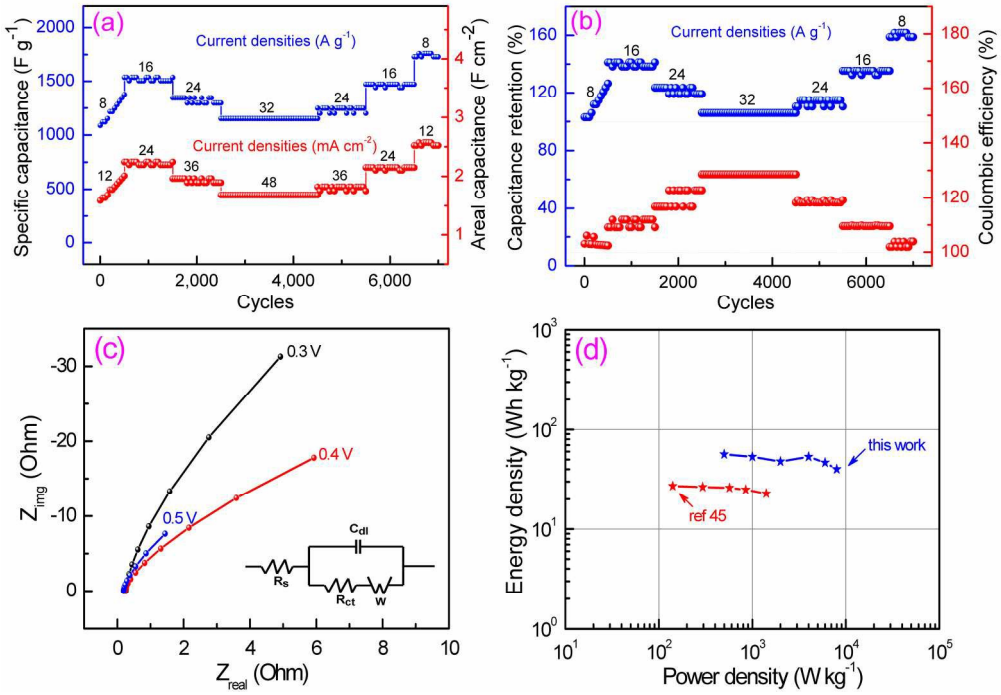

Fig. 6 (a) The cyclic performances of rGO/Ni0.3Co2.7O4 hybrid electrode at progressive current density throughout 7000 cycles. (b) Cyclic performance of capacitance retention (%) and Coulombic efficiency (%). (c) Electrochemical impedance spectra after 500 cycles of galvanostatic charge-discharge process (inset: equivalent circuit for fitting). (d) Ragone plot of as-prepared hybrid electrode along with reference.45
202x139mm (300 x 300 DPI)

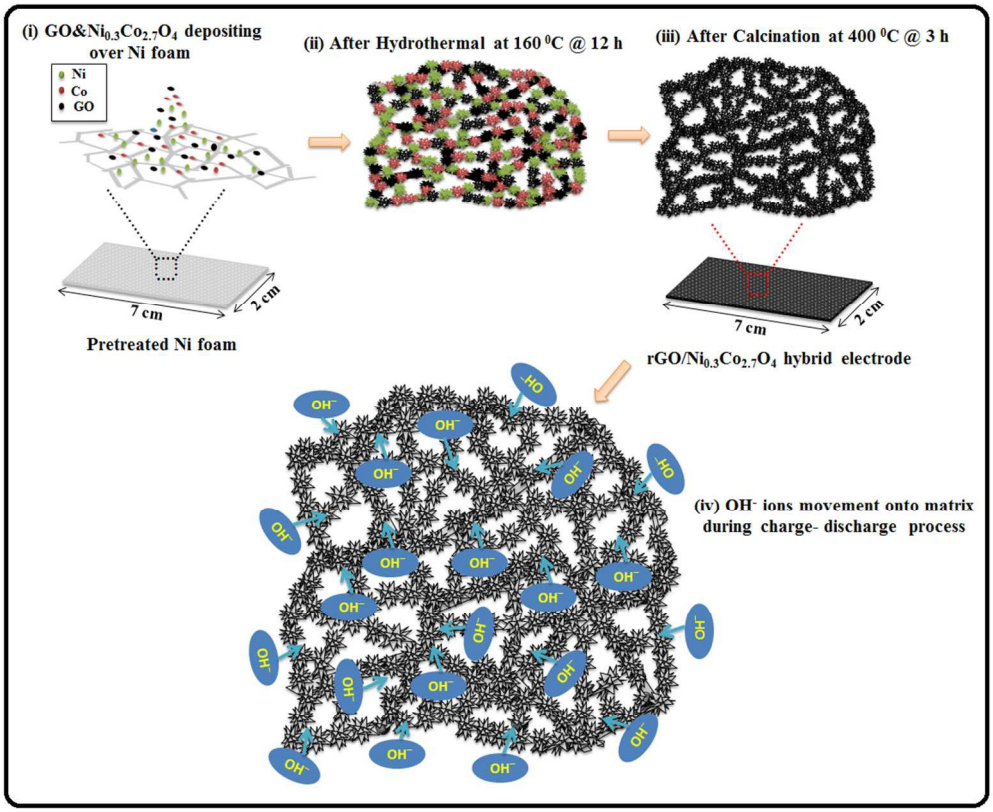

Scheme 1 (i), (ii), and (iii) Preparation illustration of microstructure rGO/Ni0.3Co2.7O4 globe artichokes hybrid electrode. (iv) OH- ions movement onto Ni foam matrix during charging and discharging.
308x253mm (96 x 96 DPI)

3D microstructured globe artichokes of rGO/$Ni_{0.3}Co_{2.7}O_4$ composite were synthesized through hydrothermal method to contribute efficient work nature as supercapacitor electrodes.